Interfacing continuum and molecular dynamics: An application to lipid bilayers

Gary Ayton
Department of Chemistry and Henry Eyring Center for Theoretical Chemistry, 315 S. 1400 E., Room 2020, University of Utah, Salt Lake City, Utah 84112-9003

Scott G. Bardenhagen and Patrick McMurtry
Department of Mechanical Engineering, University of Utah, Salt Lake City, Utah 84112-9003

Deborah Sulsky
Department of Mathematics and Statistics, University of New Mexico, Albuquerque, New Mexico 873131

Gregory A. Voth
Department of Chemistry and Henry Eyring Center for Theoretical Chemistry, 315 S. 1400 E., Room 2020, University of Utah, Salt Lake City, Utah 84112-9003

(Received 27 October 2000; accepted 24 January 2001)

A new methodology is presented for interfacing atomistic molecular dynamics simulations with continuum dynamics, and the approach is then applied to a model lipid bilayer system. The technique relies on a closed feedback loop in which atomistic level simulations are coupled with continuum level modeling. This approach allows for the examination of the *trans*-temporal and *trans*-spatial phenomena that occur in many biological systems, and nonequilibrium molecular dynamics are used to calculate the relevant transport coefficients that are required at the continuum level. It is found that for the membrane system there is significant information transfer across disparate spatial and temporal regimes, resulting in significant nonlinear behavior. © *2001 American Institute of Physics.* [DOI: 10.1063/1.1356001]

I. INTRODUCTION

There are currently a number of computer simulation techniques employed in the modeling of biological systems, ranging from molecular-level simulations (see, e.g., Refs. 1 and 2), to parameterized and phenomenological nonlinear differential equation models, to models based on bioinformatics.[3] The diversity of the techniques arises partly from the disparate time- and length-scales that are often observed in biological assemblies. There are many examples of biostructures, for example DNA strands, that must in principle be modeled at both the atomistic and continuum level in order to fully examine the system with computer simulation. The ''width'' of the DNA strand exists in a microscopic temporal/spatial regime, whereas the ''length'' is macroscopic in both length- and time-scale. Other biostructures, for example cell membranes, exhibit similar characteristics.

A drawback of using these simulation techniques separately is the absence of any direct micro-to-macro interfacing where molecular level events can interact with cellular-level ''macroscale'' phenomena and vice versa. Even the largest atomistic level simulations, taking months of computational time, do not begin to approach the time scales required to model cellular-level processes. Furthermore, the most detailed nonlinear equation cannot explicitly model molecular-level interactions if the information from such interactions is not properly incorporated. In order to completely describe such systems, some sort of linkage, or information transfer, between these disparate length and time scales is required.

In this paper we report a simulation method that has the capability of spanning micro-to-macro time/length regimes, which in essence provides a direct interface between molecular dynamics and continuum mechanics. Molecular dynamics simulations presently can model systems on the order of up to 10^5 atoms for time scales on the order of nanoseconds. Continuum level simulations that are traditionally used in engineering fields operate in macroscopic time- and length-scales or larger, but usually do so at the expense of explicit molecular level detail and structure. As shown in the present work, these two techniques can be interfaced into a closed feedback loop that essentially ''links'' the two time/space regimes.

Briefly, many of the parameters and coefficients that appear in the continuum level equations of motion (known as *constitutive coefficients* or *transport coefficients*) are averages of complex microscopic scale interactions and contain all the information of the properties of the material. Thus the micro-to-macro dynamical ''link'' can in principle be entirely contained within the transport coefficients themselves. If the relevant transport coefficients required for a continuum level simulation are calculated from a detailed atomistic model, one can essentially ''jump'' from the atomic spatial/temporal regime to the macroscale. Conversely, quantities like the density are inherently *macroscopic* in nature. Thus, if the density for an atomistic scale simulation is obtained from the calculated density in a corresponding continuum level simulation, we can essentially perform the reverse time/space ''jump.'' The combination of these two input–output sets results in a closed feedback loop between the microscale and macroscale temporal and spatial regimes.

Significant micro-to-macro feedback seems necessary in the context of cell membranes. For example, there is significant evidence[1,2] that the material properties of a membrane can be altered by small concentrations of nonmembrane particles (for example cholesterol). Also, in an earlier communication,[4] it was found that the material properties of even simple model microscopic membranes are very sensitive to changes in density, and that significant information transfer across micro-to-macro time- and length-scales can be observed.

For the present paper, we will both more fully elaborate and extend our methodology (as presented in a preliminary fashion in Ref. 4) and then apply it to a reductionist model for a lipid bilayer. In the preliminary work in Ref. 4 a membrane was modeled at the microscopic level using a ''toy'' model where a random solid of Lennard-Jones atoms was linked by a network of random harmonic ''spring-bonds.'' With this simple model, solvent effects, membrane rupture, and possible density induced phase transitions, all applicable to real membrane systems, were not possible. For the present paper, we have developed a significantly more realistic, but still computationally efficient, bilayer model that is composed of the membrane as well as solvent particles. The stability of the membrane is thermodynamic, and it is best described as a lyotropic (concentration dependent) liquid crystal. Applications of the methodology to realistic membranes are presently underway.

The paper will be divided into several sections. In Sec. II the computational methodology including the continuum level simulation technique known as the Material Point Method (MPM) as well as the microscopic method of nonequilibrium molecular dynamics (NEMD) will be described. Also in this section the description of how NEMD and MPM are interfaced into a unified micro-to-macro simulation methodology will be presented. In Sec. III, details of the application to a microscopic membrane bilayer will be discussed, and in Sec. IV results of the NEMD/MPM simulation interface will be presented. Conclusions are given in Sec. V.

II. COMPUTATIONAL METHODOLOGY

A. Continuum level simulation and the material point method

For those more familiar with microscopic level simulations (molecular dynamics), some aspects of continuum level simulation may seem similar; however, one must keep in mind that there are no independent ''particles'' and likewise the kinetic energy at some region is not to be directly associated with temperature. In a continuum level simulation, the motion of any point is given by a continuous function defined throughout the computational domain. For a numerical solution, the material is discretized into a finite number of connected regions. The continuum level simulation technique known as MPM, a numerical technique for solving large-deformation problems in continuum mechanics,[5–7] is now described.

Consider a material with spatial dimensions that are macroscopic (e.g., mm) and with dynamics existing in a macroscale temporal regime (e.g., ms). At any point in the material at any time, at the continuum level, the equation of motion solved via MPM is given by

$$\nabla \cdot \underline{\underline{\sigma}} + n\mathbf{F} = \rho \mathbf{a}, \tag{1}$$

where $\underline{\underline{\sigma}}$ is the stress tensor, $\mathbf{F}$ is an external force, ρ is the mass density, n is the number density, and $\mathbf{a}=\dot{\mathbf{v}}$ is the acceleration. In order to solve these dynamics, a *constitutive relation* is required that relates the stress $\underline{\underline{\sigma}}$ to the strain, or the gradient of the material displacement, at that point. For materials that exhibit elasticlike behavior, the incremental constitutive relation can be given by the relation,

$$\dot{\underline{\underline{\sigma}}} = \mathbf{T} : \dot{\underline{\underline{\epsilon}}}, \tag{2}$$

where the strain rate $\dot{\underline{\underline{\epsilon}}}$ is given by the symmetric part of the velocity (or flow) gradient

$$\dot{\underline{\underline{\epsilon}}} = \tfrac{1}{2}[(\nabla \mathbf{v}) + (\nabla \mathbf{v})^T]. \tag{3}$$

Here, $\mathbf{T}$ is the modulus tensor, and $\mathbf{v}$ is the flow, or velocity, at that point.

The MPM algorithm involves ''mapping'' material point velocities and masses to a regular grid $\mathbf{v} \rightarrow \mathbf{v}_g$, $m \rightarrow m_g$ at each time step. With the material point velocities and masses evaluated in this new representation, new lab fixed momenta are found, $\mathbf{p}_g = m_g \mathbf{v}_g$, and then integrated in time,

$$\mathbf{p}_g(t+\delta t) = \mathbf{p}(t) + \delta t \mathbf{f}, \tag{4}$$

where the force at the grid node is related to the stress, and therefore to the strain, where the strain is a function of the displacement. Once the grid momenta are found, they are ''mapped'' back to the materials points, and new masses and positions of the material points are calculated.

The mapping of properties such as mass and momenta from the material points to the lab fixed grid enables complete spatial freedom of material points. For dense fluids, liquid crystals, or gels this extension is necessary, since a material point can essentially move about the entire region. The MPM has also been recently generalized to treat thin membranes[8] by employing a constitutive relation as in Eq. (2). In the case of membranes with microscopic thickness, it is not immediately clear whether the system should be described by a solid (elastic) or fluid (viscous) constitutive relation. In the case of a fluid, the time derivative of the stress tensor does not appear in the constitutive relation, rather it is the stress tensor itself. This results from the fact that a fluid cannot support a shear and, under the appropriate boundary conditions, can relax to equilibrium after a stress is applied. Extensions to viscous, or viscoelastic, responses are also possible.

For this paper, we will restrict our study to membranes whose bulk behavior can be reasonably modeled with an elastic constitutive model. However, within the elastic regime one has considerable freedom of choice for the imposed strain rates. The exact form of $\dot{\underline{\underline{\epsilon}}}$ is largely determined by the chosen boundary conditions at the continuum level. For example, uniform stretching of a membrane requires equal strain-rates in the x and y directions. Conversely, stretching the membrane only in one direction (for example the x direction) requires explicitly specifying the boundary conditions in the y and z directions. One choice is to con-

strain the y and z directions to remain constant (constant length). This means that as the membrane undergoes extension in the x direction, it does not contract in other directions. A more realistic boundary condition for the y and z directions is one of zero stress. With these boundary conditions, the membrane is free to contract or expand as extensions and contractions occur in the x direction. Both sets of boundary conditions are easily implemented. For this paper, the MPM simulation will involve a membrane extending in one direction (the x direction), with all other dimensions held fixed. Other more advanced simulations are of course possible, and are currently being implemented.

With the above simplified model we can examine small, linear deformations in a membrane that is uniform in the y direction, infinitely thin in the z direction, and undergoes only stretching and compression in the x direction. Under the constraint of constant length in the y and z directions, Eq. (2) reduces to

$$\dot{\sigma}_x = E\dot{\epsilon}, \tag{5}$$

where $\dot{\epsilon} = \partial v_x/\partial t$, v_x is the flow field in the x-direction, and E is the modulus (which could be different from Young's Modulus). It is convenient to use the pressure tensor $\mathbf{P}$ rather than the external stress $\underline{\underline{\sigma}}$, where $\mathbf{P} = -\underline{\underline{\sigma}}$; thus the relationship between the time derivative of the pressure component and the strain rate is given by

$$-\dot{P}_{xx} = E\dot{\epsilon}. \tag{6}$$

A detailed description of the time integration algorithm that was used for the MPM simulation is presented in the Appendix. The general algorithm can be found in Ref. 5. The MPM continuum simulation technique as described will be employed to model a membrane bilayer at the continuum level and will be used in Sec. IV C. It should also be noted that the approach is general and, with some effort, can be extended in order to relax the above restrictions. These more realistic scenarios, in addition to applications to realistic biological membranes, will be the subject of future publications.

B. Nonequilibrium molecular dynamics

Classical molecular dynamics (MD) can be extended to the nonequilibrium regime by imposing an external field, force, or flux on the system.[9–11] The nonequilibrium dynamics will produce heat, due to the work being performed on the system. However, if this excess heat can be removed, the system can, under some circumstances, approach a nonequilibrium steady state. The more subtle aspects of the statistical mechanics of NEMD are discussed in detail in Ref. 9, and will not be presented here. For our purposes, NEMD is an efficient and elegant method to calculate transport coefficients, where the transport coefficient of interest is calculated in the limit that the nonequilibrium perturbation goes to zero. The advantage of this approach over equilibrium techniques for the calculation of transport coefficients (e.g., Green–Kubo time correlation functions) is that NEMD does not usually require either as long or large simulations.

1. Cyclic compression NEMD

Cyclic compression NEMD has been used to calculate the bulk viscosity of fluids, and has been very successful compared to traditional methods (e.g., Chapman Enskog).[12,13] This method can be applied to both elastic and viscous materials. The idea is to introduce an artificial volume oscillation, and then to correspondingly calculate the time derivative of the stress required to generate the oscillation. The modulus is then calculated in the limit that the imposed frequency and amplitude of the oscillation approaches zero. With cyclic compression NEMD a steady-state nonequilibrium state cannot be reached since the volume of the system is cyclically changed. Still, transport coefficients can be calculated as averages over compression cycles.

With cyclic compression NEMD we impose a dilation *rate* given by $\dot{\epsilon} = \zeta\omega\cos(\omega t)$, where ζ is the dimensionless amplitude of the oscillation, $\omega = 2\pi/\lambda$, and λ is the wavelength. The dilation can be applied to one, two, or all three of the Cartesian axes of the system. The Cartesian components that are subjected to the dilation depends on the design of the continuum level simulation. The NEMD simulation should ''match'' the MPM simulation, thus in the present case where the MPM simulation undergoes extensions exclusively in the x direction, the dilation at the NEMD level should also only occur in this direction. The boundary conditions at the MPM level (constant length, or zero stress) should also be consistent with the NEMD simulation. For the situation where a membrane undergoes stretching in the x direction with all other directions held fixed, the appropriate equations of motion can be easily formulated. For a microscopic system of N atoms each of mass m with positions $\mathbf{r}_1, \mathbf{r}_2, \mathbf{r}_3, \ldots, \mathbf{r}_N$ and conjugate momenta $\mathbf{p}_1, \mathbf{p}_2, \mathbf{p}_3, \ldots \mathbf{p}_N$ in a volume $V = L_x L_y L_z$, the appropriate equations of motion thus required to implement this dilation are given by

$$\dot{\mathbf{r}}_i = \mathbf{p}_i/m + \dot{\epsilon} r_{xi}\hat{\mathbf{i}}, \tag{7}$$

$$\dot{\mathbf{p}}_i = \mathbf{F}_i - \dot{\epsilon} p_{xi}\hat{\mathbf{i}} - \alpha\mathbf{p}_i, \tag{8}$$

$$\dot{L}_x(t) = L_x(t)\dot{\epsilon}. \tag{9}$$

Here, the force on particle i is $\mathbf{F}_i = -\nabla U$, where U is the potential of the system. Constant stress conditions in the directions not subject to the dilation require additional terms in the equations of motion similar in form to the artificial dilation terms, but are designed to maintain zero stress in the specified directions. This can be accomplished by standard constant stress algorithms.[9]

The term $-\alpha\mathbf{p}_i$ is a thermostatting term where the equation of motion for α, the thermostat multiplier, is given by Nose–Hoover feedback,[9]

$$\dot{\alpha} = \frac{1}{Q}(T_k(t) - T), \tag{10}$$

where Q is an arbitrary constant, T is the input thermodynamic temperature given by

$$T_k(t) = \frac{1}{dN}\sum_i^N p_i(t)^2/m, \tag{11}$$

and d is the dimensionality of the system. Without the dilation terms in the equations of motion, these dynamics generate the canonical ensemble at equilibrium.

The above equations of motion result in a dilation of the box-length in the x direction given by

$$L_x(t) = L_x(0) e^{\zeta \sin(\omega t)}, \tag{12}$$

which, as $\zeta \to 0$, becomes

$$L_x(t) = L_x(0)[1 + \zeta \sin(\omega t)]. \tag{13}$$

It is possible to formalize these dynamics such that Eq. (12) is sinusoidal, but this requires that the $t=0$ value of L_x, as well as the positions, are included in the equations of motion for the box length, Eq. (9). This dependence on the initial configuration in the equations of motion is not desirable.

A few comments regarding the applicability of this technique to membrane/solvent systems are in order. Cyclic compression is a boundary driven form of NEMD (as in the SLLOD algorithm for shear[9]) and as a result the entire system of both membrane and solvent particles are subjected to the nonequilibrium perturbation. The small layer of solvent particles has purposely been included in the calculation of the modulus. In systems where a membrane is immersed in a polar solvent, and the stability of the membrane is directly linked to membrane/solvent interactions, the exact interface between the membrane and the solvent is not well defined. For example, solvent particles that randomly percolate into the region dominated by membrane particles will directly affect that local region's structure and correlations. Likewise, membranes particles are free to diffuse into the surrounding solvent, and in that case, should not be considered as part of the ''membrane.''

For this work, the ''membrane'' has been defined as a region that exhibits certain mechanical properties, rather than being defined by its constituent particles. Since the cyclic compression NEMD technique implicitly affects *all* particles, this algorithm is particularly suited to this particular membrane definition. Alternatively, a NEMD technique that could perturb some particles, and not others, would be a better choice for larger systems where the solvent far from the membrane was not to be included in the calculation of the modulus. Techniques in the spirit of the so-called ''sinusoidal transverse field'' (STF) (Ref. 14) could either directly affect specific particles, or be applied in a specific region.

2. NEMD methodology for calculating the modulus, E

Once the appropriate constitutive relation is chosen (in this case an elastic constitutive model), the nonequilibrium finite frequency modulus can be found from exploiting the oscillatory behavior of the artificially induced cyclic compression. With the dilation of the system in the present case only occurring along the x direction, the constitutive relation between the time derivative the xx component of the pressure tensor $\dot{P}_{xx}$ and the dilation rate $\dot{\epsilon}$ is given by Eq. (6), repeated here for completeness, $-\dot{P}_{xx} = E\dot{\epsilon}$. In the weak amplitude and frequency regime, a dilation rate given by $\dot{\epsilon} = \zeta\omega\cos(\omega t)$ will result in a corresponding oscillation, $\dot{P}_{xx} = \dot{P}_1 \cos(\omega t)$, and thus

$$-\dot{P}_1 \cos(\omega t) = E\zeta\omega \cos(\omega t). \tag{14}$$

The coefficient, $\dot{P}_1$ can be found from a least squares minimization over the time interval $\Delta t = \lambda$ by defining the residual R,

$$R = \int_t^{t+\Delta t} [\dot{P}_{xx} - \dot{P}_1 \cos(\omega s)]^2 ds, \tag{15}$$

and by the minimization $\partial R/\partial \dot{P}_1 = 0$. The resulting expression, given by

$$\int_t^{t+\Delta t} \dot{P}_{xx} \cos(\omega s) ds = \dot{P}_1 \int_t^{t+\Delta t} \cos^2(\omega s) ds, \tag{16}$$

can be expressed in terms of P_{xx} and *not* its time derivative by integration by parts. This step greatly simplifies the calculations as, by contrast, $\dot{P}_{xx}$ contains terms involving the second derivative of the potential. For all but the simplest of potentials, this calculation is best avoided. The average value of the coefficient $\langle \dot{P}_1 \rangle$ over a series of compression cycles is then found to be

$$\langle \dot{P}_1 \rangle = \left\langle \frac{\omega^2}{\pi} \int_t^{t+\Delta t} P_{xx}, \sin(\omega s) ds \right\rangle, \tag{17}$$

and thus the modulus is given by

$$E = \lim_{\zeta \to 0, \omega \to 0} \frac{-\langle \dot{P}_1 \rangle}{\zeta\omega}. \tag{18}$$

C. Interfacing NEMD and MPM simulation methods

The idea behind interfacing MD and MPM simulations will be elaborated here. In principle, two concurrent simulations of the same system, with one in a microscopic time/length domain and one in a macroscale domain, exchange information between them such that a closed temporal and spatial feedback loop is constructed. In the context of a membrane/solvent system, the interface can be represented schematically and is shown in Fig. 1. Initial NEMD simulations are performed to find starting values of the transport coefficients required for the first MPM simulation [image (1)]. The MPM simulation evolves in time [image (2)], and the new predicted densities are used as input for a second round of NEMD calculations. New density dependent transport coefficients are then calculated [image (3)], and are subsequently used in another MPM iteration [image (4)]. This process is continued in an iterative feedback loop.

However, in practice, this feedback loop could be computationally costly, and many redundant calculations (especially at the microscopic level) would be performed. Depending on the complexity of the continuum model and the required constitutive relation, significant simplification to the feedback algorithm is possible. For this particular model, where we are interested in only the modulus E, the iterative loop as previously described can be replaced by a preconstructed interpolative table of E vs density ρ. A series of NEMD calculations can be performed, and the density dependence of E can be found before any MPM calculations are initialized. This method will work as long as the prelimi-

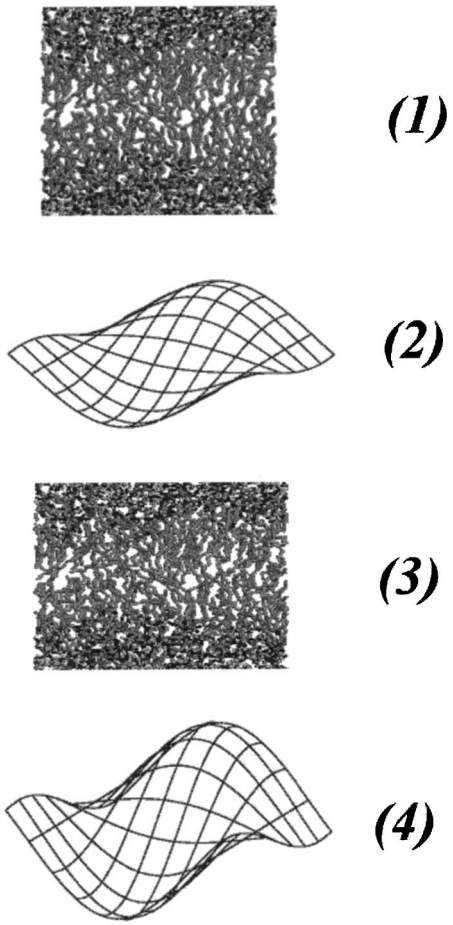

FIG. 1. A diagrammatic representation of the NEMD/MPM interface.

nary set of NEMD simulations to determine the density dependence of E spans the accessible densities sampled by MPM. For more complex systems and geometries, a more dynamic, though not directly ''on-the-fly'' feedback loop will be required where the simulation ''learns'' with time through the iterative feedback mechanism.

Also, when dealing with microscopic systems sampled over large density regimes, the possibility of a density induced phase transition must be considered. For example, at a critical low density, a stable membrane bilayer will undergo a phase transition to an isotropic mixture. Likewise at an upper density bound, the membrane may go through a liquid crystalline to solid (or gel) transition. If at the continuum level the system samples a density where a phase transition occurs (as predicted by the microscopic model), then this phase change must somehow be incorporated into the feedback mechanism. Thus a series of *equilibrium* microscopic level simulations should also be performed in order to map out those regions of the phase diagram where the membrane can be considered to be thermodynamically stable.

III. MICROSCOPIC MEMBRANE MODELS

There are various atomistic models for biological membranes ranging from very detailed atomic models of lipid bilayer systems,[1,2] to greatly simplified models (hard spherocylinders, ellipsoids of revolution) used in liquid crystal studies.[15–17] In this section we will discuss in detail the microscopic model used for our membrane bilayer. A bilayer immersed in a polar solvent, in principle, can be constructed by using models currently employed in liquid crystal computer simulations. The idea is to find a simple parameter set such that the membrane forms a stable bilayer phase, analogous to finding simple liquid crystal models that exhibit nematic or smectic phases. The choice of parameters (which includes particle shapes/sizes and charge distributions) can be selected from a reductionist examination of real bilayer membranes, and then selecting those robust interactions believed to stabilize the membrane bilayer phase. Some general characteristics that should be included in the model are:

(1) The hydrophobic–hydrophilic interactions that occurs in real lipid membranes;
(2) The elongation of the membrane molecules themselves, as well as the polar head groups.

A stable bilayer membrane surrounded by a polar solvent can be constructed using the Gay–Berne (GB) potential[18–20] generalized to a mixture formulation,[21] where mixtures of differently shaped particles can easily be modeled. The Gay–Berne potential has the ability to model particles as ellipsoids of revolution with aspect ratio, l/d, where l is the length of the particle, and d is the diameter, with a potential similar in spirit to a Lennard-Jones potential. The potential has been parameterized such that the attractive well depth varies with the orientation *and* position of the particle. The current parameterization[18] results in low energy configurations that favor side-by-side parallel configurations, similar to the behavior of a site model of Lennard-Jones atoms resulting in the same aspect ratio.

A Gay–Berne membrane/solvent model: In this section the computational details associated with the lipid bilayer model will be discussed. In microscopic molecular dynamics simulations, the total energy of the system U is usually expressed as a sum of pair potentials U_{ij} over the N particles in the system, $U=\Sigma_{i<j}^{N}U_{ij}$. The interaction energy between two molecules i and j can be written as

$$U_{ij}=U_{\mathrm{GB}}(\hat{\mathbf{r}}_{ij},\hat{\mathbf{u}}_i,\hat{\mathbf{u}}_j)+U_{qq}, \tag{19}$$

where $U_{\mathrm{GB}}(\hat{\mathbf{r}}_{ij},\hat{\mathbf{u}}_i,\hat{\mathbf{u}}_j)$ is the Gay–Berne potential,[18] and U_{qq} represents electrostatic interactions. The Gay–Berne potential is a convenient potential capable of modeling particles with spherical or ellipsoidal shapes, and can be written as

$$U_{\mathrm{GB}}(\hat{\mathbf{r}}_{ij},\hat{\mathbf{u}}_i,\hat{\mathbf{u}}_j)=4\epsilon(\hat{\mathbf{r}}_{ij},\hat{\mathbf{u}}_i,\hat{\mathbf{u}}_j)[\zeta_{ij}^{12}-\zeta_{ij}^{6}], \tag{20}$$

$$\zeta_{ij}=\frac{\sigma_0}{r_{ij}-\sigma(\hat{\mathbf{r}}_{ij},\hat{\mathbf{u}}_i,\hat{\mathbf{u}}_j)+\sigma_0}, \tag{21}$$

where the orientation of molecule i is given by the unit vector $\hat{\mathbf{u}}_i$ and the intermolecular distance between the centers of mass of particle i and j is given by $r_{ij}=|\mathbf{r}_i-\mathbf{r}_j|$. The unit vector $\hat{\mathbf{r}}_{ij}$ is given by $\hat{\mathbf{r}}_{ij}=(\mathbf{r}_i-\mathbf{r}_j)/r_{ij}$. The range parameter, $\sigma(\hat{\mathbf{r}}_{ij},\hat{\mathbf{u}}_i,\hat{\mathbf{u}}_j)$ is approximately the distance of closest approach for two identical ellipsoids i and j with aspect ratio l/d and orientations given by $\hat{\mathbf{u}}_i$ and $\hat{\mathbf{u}}_j$. This parameter is given by

$$\sigma(\hat{\mathbf{r}}_{ij},\hat{\mathbf{u}}_i,\hat{\mathbf{u}}_j)=\sigma_0\left[1-\frac{\chi}{2}\left[\frac{(\hat{\mathbf{r}}_{ij}\cdot\hat{\mathbf{u}}_i+\hat{\mathbf{r}}_{ij}\cdot\hat{\mathbf{u}}_j)^2}{1+\chi\hat{\mathbf{u}}_i\cdot\hat{\mathbf{u}}_j}+\frac{(\hat{\mathbf{r}}_{ij}\cdot\hat{\mathbf{u}}_i-\hat{\mathbf{r}}_{ij}\cdot\hat{\mathbf{u}}_j)^2}{1-\chi\hat{\mathbf{u}}_i\cdot\hat{\mathbf{u}}_j}\right]\right]^{-1/2}. \tag{22}$$

In this expression χ is given by

$$\chi=\frac{(l/d)^2-1}{(l/d)^2+1}. \tag{23}$$

The well-depth strength anisotropy parameter is given by

$$\epsilon(\hat{\mathbf{r}}_{ij},\hat{\mathbf{u}}_i,\hat{\mathbf{u}}_j)=\epsilon_0\epsilon_1^{\mu}(\hat{\mathbf{u}}_i,\hat{\mathbf{u}}_j)\epsilon_2^{\nu}(\hat{\mathbf{u}}_i,\hat{\mathbf{u}}_j,\hat{\mathbf{r}}_{ij}), \tag{24}$$

where $\mu=2$, $\nu=1$,[18] and $\epsilon_2(\hat{\mathbf{u}}_i,\hat{\mathbf{u}}_j,\hat{\mathbf{r}}_{ij})$ is given by

$$\varepsilon_2(\hat{\mathbf{u}}_i,\hat{\mathbf{u}}_j,\hat{\mathbf{r}}_{ij})=\left[1-\frac{\chi'}{2}\left[\frac{(\hat{\mathbf{r}}_{ij}\cdot\hat{\mathbf{u}}_i+\hat{\mathbf{r}}_{ij}\cdot\hat{\mathbf{u}}_j)^2}{1+\chi'\hat{\mathbf{u}}_i\cdot\hat{\mathbf{u}}_j}+\frac{(\hat{\mathbf{r}}_{ij}\cdot\hat{\mathbf{u}}_i-\hat{\mathbf{r}}_{ij}\cdot\hat{\mathbf{u}}_j)^2}{1-\chi'\hat{\mathbf{u}}_i\cdot\hat{\mathbf{u}}_j}\right]\right], \tag{25}$$

where

$$\chi'=\frac{1-(\varepsilon_E/\varepsilon_S)^{1/\mu}}{1+(\varepsilon_E/\varepsilon_S)^{1/\mu}}, \tag{26}$$

and the ratio of end-to-end and side-to-side well depths is given by $\varepsilon_E/\varepsilon_S$.

In this form, systems of identical ellipsoidal particles can be modeled. For mixtures, it is possible to extend the model,[21] and in the case of a mixture of ellipsoidal and spherical particles, Eq. (22) has to be modified. In the case that, for example, the ith particle is spherical, then $l_i=d_i=d$ and the appropriate range parameter is given by

$$\sigma(\hat{\mathbf{r}}_{ij},\hat{\mathbf{u}}_j)=\sigma_0\left[1-\frac{\chi}{\alpha^2}(\hat{\mathbf{r}}_{ij}\cdot\hat{\mathbf{u}}_j)^2\right]^{-1/2}, \tag{27}$$

where

$$\frac{\chi}{\alpha^2}=\frac{l_j^2-d_j^2}{l_j^2+d^2}. \tag{28}$$

Note that there is no unique form for the energy parameter. The simplest option for a sphere–ellipsoid interaction is to simply make the energy parameter a constant. The Gay–Berne potential reduces to the familiar Lennard-Jones potential for fluids of spherical atoms. The cross interaction between ellipsoidal particles and spherical particles was modified to promote demixing by omitting the attractive ζ_{ij}^6 term in the potential. An Ewald summation[22] was used to calculate the electrostatic component of the energy, U_{qq}, and the method used is described in detail in Refs. 23 and 24, along with the relevant expression to calculate the components of the pressure tensor **P**.

With the model as defined, the membrane bilayer system was constructed from the following particles and is shown in Fig. 2. The membrane particles were ellipsoids of revolution of length 20 Å and diameter 5 Å. A dipolar charge distribution embedded within a sphere of diameter 5 Å was placed at one end of the GB particle, making one end of the particle ''polar'' and one end nonpolar. The charge distribution was constructed by placing a positive charge $q_+=0.705$ esu and a corresponding negative charge $q_-=-0.705$ esu at a distance of $l=0.5$ Å from the center of the terminal sphere such that the resulting dipole moment $\mu=ql$ was perpendicular to the long axis of the ellipsoid. The solvent particles were modeled with a Lennard-Jones potential (or equivalently GB particles with aspect ratio equal to 1) with a charge distribution identical to the membrane particles'.

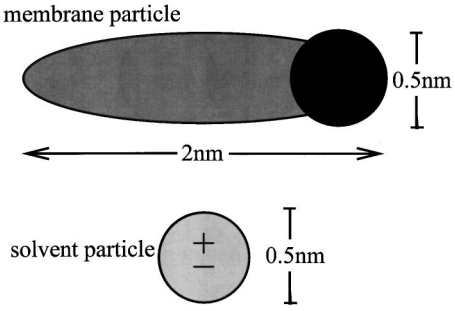

FIG. 2. The geometry and charge distributions for the two types of particles used in the Gay–Berne membrane bilayer/solvent simulations.

IV. RESULTS

The results will be divided into two sections: equilibrium MD results and nonequilibrium NEMD results. The equilibrium simulations were used to establish the densities where the membrane bilayer was thermodynamically stable with respect to isotropic, gel, and solid phases. The NEMD runs were then used to calculate the density dependent modulus E.

A. MD simulation

A series of equilibrium runs were performed to find the high density and low density bounds where the membrane was stable. Above the high density bound, the membrane was in a gel, or solid phase. Below the low density bound, the membrane decomposed into a phase that appears to be an isotropic mixture of solvent and membrane particles. The results are presented first with three simulation snapshots of the membrane. The highest density system is shown in Fig. 3(a) at a density of $\rho^*=N\sigma^3/V=0.4622$. Here, N is the *total* number of particles, both solvent and membrane, V is the volume of the simulation box, and $\sigma=d=5$ Å is the diameter of the particles (the same for both solvent and membrane). For clarity, the membrane particles are drawn as spherocylinders with a diameter of 0.25 Å and likewise the solvent particles are also not drawn to scale. With the shaded caps on the membrane particles designating the location of the terminal dipole, one can see that the polar tips of the membrane particles are in direct contact with the polar solvent. Likewise, the opposing nonpolar end of the membrane particles tend to point away from the solvent. Simulation runs of 100 ps were performed to ensure that the membrane remained thermodynamically stable. A careful look at Fig. 3(a) shows that some membrane particles are not bound within the membrane but reside in the polar solvent. There is no fundamental reason that membrane particles must remain bound within the bilayer. An indication of the stability of the bilayer membrane phase relative to the isotropic mixture

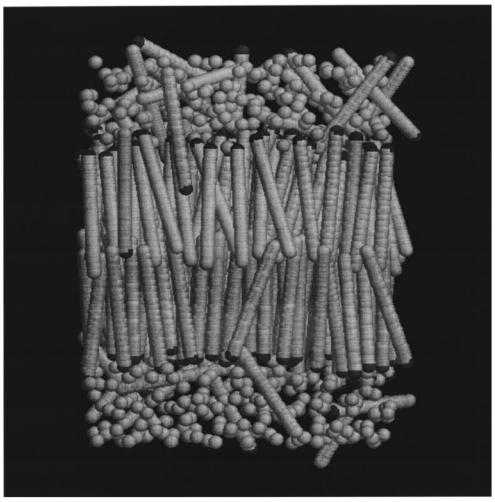

(a)

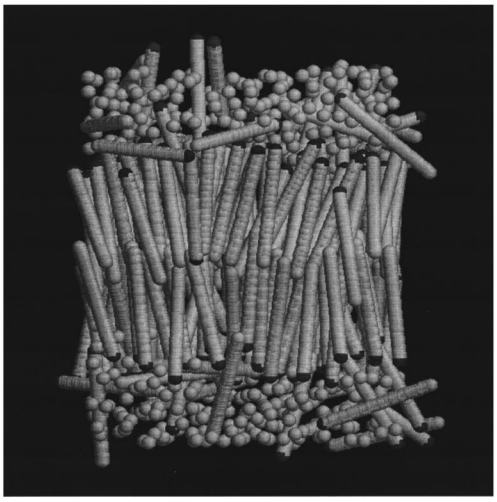

(b)

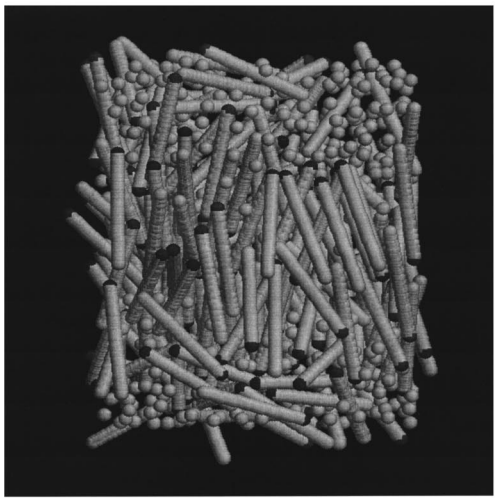

(c)

FIG. 3. Panel (a) is a computer simulation snapshot of the membrane bilayer at the highest density, $\rho^*=N\sigma^3/V=0.4622$. For clarity the membrane particles have been represented as spherocylinders of length 20 Å and width 2.5 Å. The shaded tip of the membrane particle designates the location of the dipolar charge distribution. Also for clarity, the solvent (Lennard-Jones atoms) are not drawn to scale. In this image the membrane bilayer is thermodynamically stable, but is also not frozen. Panel (b) is a snapshot at a lower density, $\rho^*=N\sigma^3/V=0.4388$, and the orientational order of the membrane is not as strong. Panel (c) is a snapshot at a low density, $\rho^*=N\sigma^3/V=0.4188$, where the system is approaching an isotropic mixture of membrane and solvent particles.

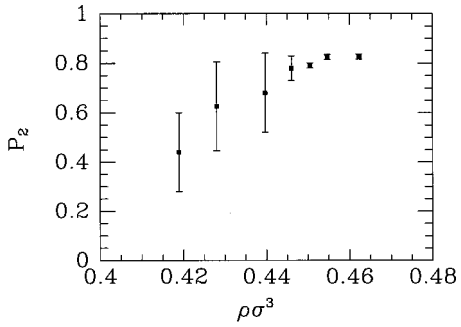

FIG. 4. The P_2 order parameter for the membrane particles vs reduced density, $\rho^*=N\sigma^3/V$.

phase can be found by calculating the P_2 order parameter for the N_M membrane particles. The time-averaged P_2 order parameter is defined as[25]

$$P_2=\frac{1}{N_M}\left\langle \sum_{i=1}^{N_M}\frac{1}{2}(3\cos^2\theta_i-1)\right\rangle_t, \tag{29}$$

where $\theta_i=\hat{\mathbf{u}}_i\cdot\mathbf{d},\mathbf{d}$ the director associated with the membrane particles, $\hat{\mathbf{u}}_i$ is a unit vector along the symmetry axis of the membrane particle, and $\langle\cdots\rangle$ represents a time average. For this system, an isotropic fluid mixture of membrane particles immersed in the solvent would correspond to $P_2\sim 0$, while an ordered membrane bilayer will have $P_2\sim 0.8$ allowing for fluctuations in particle orientations with respect to the director. The P_2 order parameter, as defined, gives no structural information; that is it cannot describe the degree of spatial order of the membrane bilayers. However, since the degree of orientational order of the particles is directly correlated to the degree of spatial order, the P_2 order parameter is an adequate measurement of membrane stability relative to the isotropic mixture phase.

A plot of the P_2 order parameter versus density is given in Fig. 4. For this density, $\rho^*=N\sigma^3/V=0.4622$, $P_2\sim 0.81$, indicating a high degree of orientational order in the membrane bilayer. The mean square displacement perpendicular to the director, $\langle|\mathbf{r}_{xy}(t)-\mathbf{r}_{xy}(0)|^2\rangle$, $\mathbf{r}_{xy}=r_x\hat{i}+r_y\hat{j}$ (in this case, the director is taken to be fixed and along the z axis) is shown in Fig. 5, also indicates that the membrane is not frozen, and that there is significant diffusion. For this density

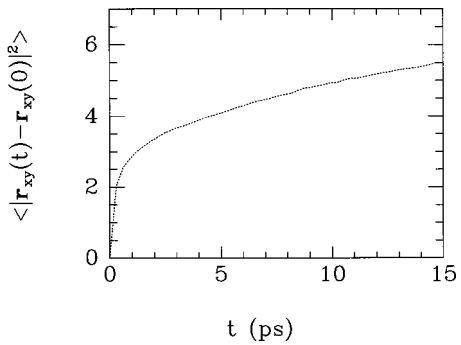

FIG. 5. The mean square displacement of the membrane particles within the plane of the membrane, $\langle|\mathbf{r}_{xy}(t)-\mathbf{r}_{xy}(0)|^2\rangle$, for the highest density system, $\rho^*=N\sigma^3/V=0.4622$.

the combination of the P_2 order parameter and the mean square displacement within the plane of the membrane suggests that (1) the membrane is stable with respect to the isotropic mixture and (2) is in a fluid vs solid phase.[26]

The next simulation snapshot [Fig. 3(b)] corresponds to a lower density, $\rho^* = N\sigma^3/V = 0.4399$, and a visual inspection of the image shows that the orientational correlations between the membrane particles are weaker, and that the spatial structure of the bilayer is less well defined. Still, the terminal dipole moments of the particles generally interact directly with the polar solvent, and the inner core of the membrane remains nonpolar. The P_2 order parameter for this density is $P_2 \sim 0.65 \pm 0.2$, consistent with the qualitative observations from Fig. 3(b). For this finite-sized system, and without more detailed calculations, it is difficult to determine the exact location, and thermodynamic order, of the phase transition between the membrane bilayer and the isotropic mixture of membrane and polar solvent particles. The P_2 order parameter from Fig. 4 suggests that this density corresponds to the low density stability limit of the membrane bilayer. More detailed constant pressure and temperature (NPT) calculations with larger system sizes could pinpoint the location of the transition with greater accuracy, but for this study we are only interested in the approximate lower density limit for the membrane bilayer, corresponding to $\rho^*_{\mathrm{min}} \sim 0.44$.

The low density near-isotropic mixture is shown in Fig. 3(c) ($\rho^* = N\sigma^3/V = 0.4188$), where clearly the structural integrity of the membrane is gone, and the system is approaching a random mixture of membrane and solvent particles. There is little or no preferred orientation of the membrane particles ($P_2 \sim 0.4$), within finite size effects.

From these preliminary equilibrium calculations, the density range where the membrane bilayer can be assumed to be stable can be roughly determined. The exact order of the transition from membrane bilayer to isotropic mixture is not known (i.e., whether it is first order, second order, or higher). In all likelihood the transition is at best weakly first order, and possibly higher. At the highest density sampled, the membrane is still fluid, at least in terms of the diffusion of the membrane particles within the plane of the bilayer. The working density range to be used in subsequent MPM simulations was thus taken to be $\rho^*_{\mathrm{min}} = 0.440$ to $\rho^*_{\mathrm{max}} = 0.462$.

B. NEMD simulation

We will begin the discussion of the NEMD simulations with Fig. 6, where the instantaneous value of P_{xx} for the high density system, $\rho^* = N\sigma^3/V = 0.4622$ vs time t is shown. Also shown is the dilation rate, $d\epsilon/dt$, for the lowest frequency oscillation, $\omega = 0.1256\,\mathrm{ps}^{-1}$. There is no means of knowing beforehand whether or not the response of the membrane to the artificially imposed dilation rate will be elastic, viscous, or neither. As previously described, an elastic response corresponds to a constitutive relation given by Eq. (5), whereas a viscous response traditionally associated with isotropic Newtonian fluids would be given by $\sigma = \eta\dot{\epsilon}$, where η is a viscosity, since fluids cannot support a strain.[9] By construction, the boundary conditions chosen for this dilation correspond to oscillations in the x direction only, and there is no variation in the perpendicular y direction. In other words, the membrane is not allowed to contract in the y direction due to extension in the x direction. As previously mentioned, other boundary conditions could also be employed.

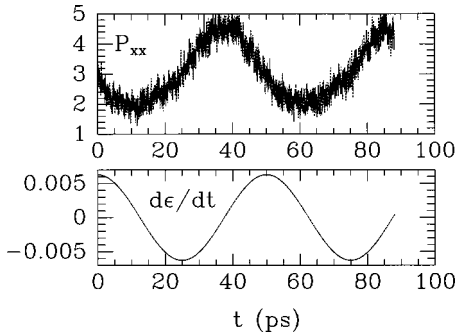

FIG. 6. The instantaneous value of P_{xx} for the high density system, $\rho^* = N\sigma^3/V = 0.4622$ vs time t. Also shown is the dilation rate, $d\epsilon/dt$ for the lowest frequency oscillation, $\omega = 0.1256$. P_{xx} exhibits a sinusoidal variation in time, while $d\epsilon/dt$ has the imposed cosine form.

To ensure that the proposed elastic constitutive model given by Eq. (6) is valid, the response of the P_{xx} component of the pressure tensor was monitored along with the imposed oscillation. Clearly, from Fig. 6, with a dilation rate with a cosine behavior, P_{xx} is sinusoidal with no visible phase shift, indicating that the response is purely elastic with no out of phase components. This is an important point: the constitutive relation proposed in Sec. II A must be validated by examining the natural response of the system before it is employed in a continuum level model. Cyclic compression NEMD affords a means of monitoring the response of the system to the artificial dilation without assuming the form of the constitutive model. This elastic behavior is typical of all systems studied within the range ρ^*_{min} to ρ^*_{max}. The elastic response of this system can be attributed to its high density combined with the fact that the bilayer structure induces two-dimensional spatial correlations. It is well known that fluids of two-dimensional disks[25] exhibit strong solidlike finite-range spatial correlations. Thus even though this phase has nonzero diffusion within the plane of the membrane, it retains strong solidlike spatial correlations, and furthermore, its response to changes in area is more indicative of an elastic solid. It is possible that a model that can support a stable bilayer at lower densities may have a viscous, or viscoelastic, response. In that case, a more general constitutive relation than in Eq. (5) would be required.

The model membrane for this study is as described in Sec. III A. A total of seven different densities were examined: $\rho^* = 0.4622$, 0.4546, 0.4505, 0.4460, 0.4397, 0.4280, and 0.4189. Each simulation was started from a lattice of 200 membrane particles (ellipsoids of revolution with aspect ratio $l/d = 4$) arranged in a bilayer, with 400 solvent particles (dipolar Lennard-Jones atoms with diameter equal to the short axis of the membrane particles). The membrane bilayer was initially composed by an array ($x \times y \times z$) of $10 \times 10 \times 2$ particles. As the diameter of the solvent particles was chosen to be equal to the width of the membrane ellipsoids, a similar

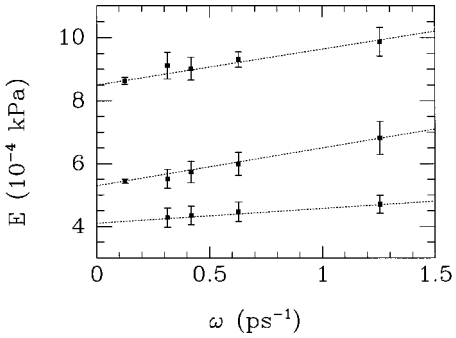

FIG. 7. The nonequilibrium modulus E plotted vs dilation frequency ω for three selected densities corresponding to $\rho^*=0.4662$, 0.4505, and 0.4189. For each point, an extrapolation to zero frequency gives a value of the zero frequency modulus.

array of solvent particles was placed above and below the membrane. Briefly, the NEMD simulations were performed by first running an equilibrium simulation of $N=600$ molecules for a time of 100 ps, and then subjecting the system to a series of 40–100 nonequilibrium cyclic compressions in the x-direction.

For each density sampled, two different amplitudes corresponding to $\zeta=0.25$ and 0.125, and five different frequencies ranging from $\omega=0.125\,\mathrm{ps}^{-1}$ up to $\omega=1.25\,\mathrm{ps}^{-1}$ were used. The magnitude of the amplitudes was less than 5% of the original cell size, and the shortest frequency corresponded to a wavelength of $50\,000dt$, where $dt=0.001$ ps. In Fig. 7 the modulus E is plotted vs dilation frequency ω for three selected densities corresponding to $\rho^*=0.4662$, 0.4505, and 0.4189. The nonequilibrium values of E for all three densities increase linearly with increasing ω, with the highest density runs exhibiting the greatest slope. For each point, an extrapolation to zero frequency gives a value of the zero frequency modulus.

The extrapolated values of E can be plotted vs $\rho^*=N\sigma^3/V$. In Fig. 8 the variation of the zero frequency modulus E with respect to the density is clearly shown. There appears two be two distinct regions corresponding to the regime where the membrane is stable and E is a linear function of ρ^* (designated as the region to the right of the gray line), and to the regime where the membrane may be

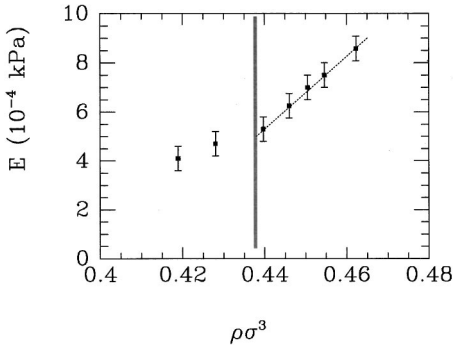

FIG. 8. The density dependence of the modulus, E. The region designated by the dashed line corresponds to the density regime where the membrane was found to be thermodynamically stable. Only this region was employed in the continuum level simulations.

TABLE I. Initial parameters used for the MPM membrane–spring simulation. The mass M corresponds to the mass of a material point.

L (mm)	A (mm^2)	E ($kg\,m^{-1}\,s^{-2}$)	M (μg)	g [mm$(ms)^{-2}$]
0.30	0.001	8.62×10^4	0.02788	9.81×10^{-3}

close to a phase transition to an isotropic mixture (to the left of the gray line). When this figure is compared to Fig. 4, it appears that the two different branches in Fig. 8 are correlated to the density dependence of the P_2 order parameter. In the regions where $P_2\sim0.8$, E changes rapidly and linearly with ρ^*. In the regions where $P_2<0.8$ and the membrane is becoming thermodynamically unstable, the slope of E vs ρ^* is less. The exact density dependence of E in the region below ρ^*_{min} is difficult to determine due to system size effects. A detailed analysis of the order, and location, of the membrane to isotropic mixture transition is required in order to make definitive conclusions at these lower densities. For that reason, only the high density branch was used for the dynamic feedback regime allowed in the MPM simulations. Above and below these densities, the liquid crystalline integrity of the membrane was not clear.

C. MPM simulation

The results from Fig. 8 can now be used as initial input for a MPM continuum level membrane simulation. Recall that for this problem the micro-to-macro interface is accomplished by means of a preconstructed E vs ρ^* table that has been *uniquely* determined for the chosen membrane model from the atomistic NEMD simulations. The upper and lower density bounds for the MPM simulation were chosen to correspond to the densities where the membrane bilayer was estimated to be stable.

The MPM simulation was set up to model a macroscopic membrane that was anchored at one end, with a weight attached to the other. Under the force of gravity, the membrane extends and the weight bounces. For this experiment, a membrane of length 0.3 mm and cross-sectional area of 0.001 mm^2 was chosen. Ten material points and four grid nodes where placed on the membrane, and the tenth material point (the one at the bottom) was given a mass 5000 times greater than the other material points to model the weight attached to the end of the membrane. The initial value of the modulus was $8.62\times10^4\,\mathrm{kg\,m^{-1}\,s^{-2}}$ corresponding to a reduced density of $\rho^*=0.4622$. Further details are summarized in Table I, and a diagram of the continuum level model is shown in Fig. 9. This particular model is being studied here as a demonstration of the NEMD/MPM feedback loop. Other, more realistic, continuum level simulations can be constructed, but for the present purposes this continuum problem is attractive in that it has an analytic solution in the density-independent case, and it clearly shows the effects of micro-to-macro feedback (see below).

In Fig. 10 is presented the results for the dynamic feedback interface between a microscopic level simulation with the continuum-level MPM model. The curves in the plot track the displacement of the ''heavy'' material point over time. Note that the spatial displacement is now in millime-

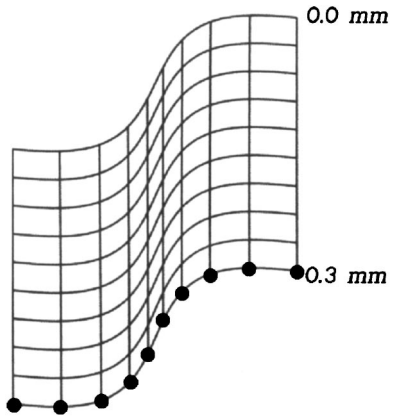

FIG. 9. A diagrammatic representation of the continuum level membrane.

ters, and the time is in milliseconds. Recall that the modulus was originally calculated using a microscopic scale simulation on a length-scale on the order of nanometers and time scales on the order of picoseconds. Thus, not only have we effectively jumped both spatial and temporal scales, but more importantly, we have actually *interfaced* micro- and macroregimes via the density dependence of the modulus. An informative calculation is to determine the system size, and computational time, that would be required to model this simple spring experiment using a detailed microscopic model with no bridging to the continuum level MPM simulation. In order to match the chosen dimensions of the MPM simulation, a microscopic simulation of 1.0×10^{15} molecules running for 1.0×10^{10} ps would be required. Present atomic-level simulation capabilities are not anywhere near being capable of handling such simulations. In contrast, with NEMD/MPM feedback, the MPM calculation takes about a minute on a workstation (SGI 02, R5000, 200 mHz), while each NEMD modulus point takes about 10 h to calculate.

The actual point where the microscopic information is transferred to the continuum level simulation occurs within the time integration component of the MPM algorithm. When the density at a specific material point is updated in the time integration, the value of E, as shown in Fig. 8, is employed in the constitutive relation,

$$\dot{P}_{xx}(t) = -E[\rho(t)]\dot{\epsilon}(t). \tag{30}$$

As the spring-membrane extends, and its length increases, the density within the membrane decreases. From Fig. 8, it is seen that in the sampled density regime, E decreases linearly with ρ, meaning that the membrane becomes ''softer'' as it extends. The result is evident in Fig. 10, where it is seen that the membrane extends slightly farther when micro-to-macro feedback is included (long-dashed line) vs the constant E case (solid line).[27]

The short-dashed line in Fig. 10 that terminates just before $t=2$ ms is the oscillation induced when a weight 8000 times the mass of a material point is used. With this weight, the membrane extends such that the density goes below $\rho^*_{\min}$ and the membrane enters a regime where a phase transition to an isotropic mixture occurs. There is no way that the continuum level simulation could know that the membrane was undergoing a density induced phase transition, so only when microscopic information is included, can the MPM simulation incorporate phase transitions or membrane rupture. Presumably, with more detailed microscopic level NEMD calculations, it may be possible to formulate a new constitutive relation for situations below $\rho^*_{\min}$, but without further simulations, the MPM simulation cannot be allowed to access that density regime. Thus, when too much weight is put on the membrane such that it extends past $\rho^*_{\min}$, the membrane is assumed to have gone through a phase transition, and it has either ruptured or broken down.

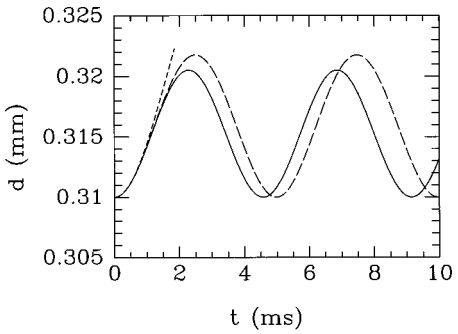

FIG. 10. The MPM simulation for the membrane bilayer system. The solid line represents the gravity induced oscillation without dynamic feedback, while the long-dashed line is the result when micro-to-macro interfacing occurs. The slightly longer extension with micro- macro- dynamic feedback results from the membranes density dependent modulus. The short-dashed line is the result when too much weight is attached to the membrane, and the membrane is no longer stable.

V. CONCLUSIONS

We have examined the behavior of a membrane bilayer/solvent system using a new micro-to-macro dynamical feedback simulation technique. With this method, two simulations at different time and length scales are interfaced into a unified simulation methodology. The interface is accomplished via an information transfer where selected material properties (transport coefficients) and state parameters (density) are calculated in one spatial/temporal regime and then used as initial input in another. What results is a closed feedback loop.

The membrane/solvent system was constructed as a reductionist model of a biological lipid bilayer system. It was found that in the density regime, where the bilayer is thermodynamically stable, the modulus of the system that describes extension within the plane of the membrane varies sharply with density. When interfaced with a continuum level simulation, it was also found that the micro-to-macro dynamic feedback interface results in significant changes compared to the case when the feedback is not employed. Further, when combined with equilibrium results used to determine the thermodynamic stability density range of the membrane, the micro-to-macro interface can be used to predict membrane rupture.

By employing the present dynamic feedback methodology we are able, in essence, to introduce microscopic information into continuum level simulations and, more impor-

tantly, we are able to examine systems well beyond the size and time scales currently accessible by atomistic MD simulation techniques.

ACKNOWLEDGMENT

This research was supported in part by the University of Utah Research Foundation Incentive Seed Grant Program.

APPENDIX: THE MATERIAL POINT METHOD ALGORITHM

In this Appendix we will discuss the MPM numerical technique, with focus on those aspects that involve the NEMD/MPM interface. In MPM a material is discretized into a finite number of material points. Additionally a grid, or mesh, is used as a ''scratch pad'' for the solution of governing equations. The material points are free to move through the grid and possess the following attributes:

(1) mass;
(2) velocity;
(3) stress ($\underline{\underline{\sigma}}$ in general, or $-P_{xx}$ in this model).

In fact, it is the transfer of information between material points and grid that is the essence of the method. In 1D, the transformation of quantities between the material points (where a material point p is located at x_p), and the lab fixed grid nodes (where the ith grid node is located by x_i) is handled by the grid nodal basis function $N_i(x_p)$. For the geometry of interest, where a spring membrane is in the x-direction, we can write the nodal basis function in terms of the grid node spacing, δx as

$$N_i(x_p)=1-\left|\frac{x_i-x_p}{\delta x}\right|, \quad x_i-\delta x<x_p<x_i+\delta x$$
$$=0, \qquad \text{otherwise.} \tag{A1}$$

In general, any function of the material points $f(x_p)$ can be transformed to a function of the grid nodes, $f(x_i)$. The transformation can be more easily understood in the context of more familiar transforms, such as a Fourier transform.[9] In the case where the grid node spacing, $\delta x \to 0$ and the number of material points becomes large, $N_p \to \infty$, the nodal basis functions can be represented as densities and the transformation from the material points to the grid representation can be written as

$$\tilde{f}(x)=\int dx' N_i(x') f(x'), \tag{A2}$$

and likewise for the backtransformation. Employing the nodal basis function means that evaluating gradients of $\tilde{f}$ are handled by the gradients of the nodal basis functions themselves,

$$\frac{\partial}{\partial x}\tilde{f}(x)=\int dx' \frac{\partial}{\partial x} N_i(x') f(x'). \tag{A3}$$

Thus gradients of functions under the nodal basis transformation requires only the gradient of the nodal basis function itself. The elegance of the MPM method relies on the choice of which quantities will be carried in the material point reference frame, and which ones will be in the grid node frame; a careful separation results in easily handling the derivatives of specific functions.

The algorithm consists of ten steps. A general discussion can be found in Ref. 5, and here we present the algorithm relevant to the problem of a one-dimensional spring mass problem. Consider a system of N_p material points, aligned in the x-direction, at locations x_p. A series of N_i grid nodes at locations x_i is superimposed over the material point system.

Step 1: Calculate the momenta of the material points in the grid node space. If we denote the mass of the material points as m_p, and their corresponding velocity as v_p, then the momenta in the grid node representation is given by

$$(mv)_i=\sum_{p=1}^{N_p} N_i(x_p) m_p v_p, \tag{A4}$$

where the nodal basis function has been previously defined.

Step 2: Calculate m_i, the mass in the grid node representation,

$$m_i=\sum_{p=1}^{N_p} N_i(x_p) m_p. \tag{A5}$$

Step 3: Calculate v_i, the velocity in the grid node representation,

$$v_i=(mv)_i/m_i. \tag{A6}$$

Step 4: Evaluate the forces, f_i at the grid nodes. This is the first application of the derivatives of the nodal basis function. If the stress at the material points is given by σ_p, and the volume associated with each material point (in this geometry this is simply given by the distance between material points) is V_p, then f_i is given by

$$f_i=-\sum_{p=1}^{N_p} V_p \frac{\partial N_i(x_p)}{\partial x_p}\sigma_p. \tag{A7}$$

Note that to evaluate the forces at the grid nodes, only the derivative of the nodal basis function is required.

Step 5: Calculate the accelerations at the grid nodes,

$$a_i(t+\delta t)=\frac{f_i}{m_i}. \tag{A8}$$

Step 6: Predict the new velocities at the grid nodes. The explicit time dependence is now included, and the predicted velocities are denoted by an asterisk,

$$v_i^*(t+\delta t)=v_i(t)+a_i(t+\delta t)\,\delta t. \tag{A9}$$

Step 7: Calculate the strain-rate at the material points using the predicted velocities at the grid nodes,

$$\dot{\epsilon}_p=\frac{\partial v_p^*(t+\delta t)}{\partial x_p}=\sum_{i=1}^{N_i}\frac{\partial N_p(x_i)}{\partial x_p} v_i^*(t+\delta t). \tag{A10}$$

Step 8: Integrate the stress at the material points by employing the constitutive relation

$$\dot{\sigma}_p(t)=E(t)\,\dot{\epsilon}_p(t), \tag{A11}$$

where $-P_{xxp}(t)=\sigma_p(t)$ and we explicitly include the possibility of a time dependent modulus, $E(t)$. This is the step where the microscopic information is included via the density dependence of the modulus.

Step 9: Calculate the velocities and accelerations in the material point representation,

$$a_p^*(t+\delta t)=\sum_{i=1}^{N_i} N_p(x_i)a_i^*(t+\delta t). \tag{A12}$$

Step 10: Update the material point positions and velocities using

$$\begin{aligned} r_p(t+\delta t)&=r_p(t)+v_p^*(t+\delta t)\,\delta t,\\ v_p(t+\delta t)&=v_p(t)+a_p^*(t+\delta t)\,\delta t, \end{aligned} \tag{A13}$$

and then return to step 1.

[1] K. Tu, M. L. Klein, and D. J. Tobias, Biophys. J. **75**, 2147 (1998).
[2] A. M. Smondyrev and M. L. Berkowitz, Biophys. J. **77**, 2075 (1999).
[3] In the field of bioinformatics, one can find several examples of ''virtual'' simulations of such things as living organisms, human organs, etc. These efforts are presently even being commercialized (see, e.g., http://www.physiome.com/default.html, http://www.entelos.com/).
[4] G. Ayton, S. Bardenhagen, P. McMurtry, D. Sulsky, and G. A. Voth, IBM J. Res. Dev. (to be published).
[5] D. Sulsky, Z. Chen, and H. L. Schreyer, Comput. Methods Appl. Mech. Eng. **118**, 179 (1994).
[6] D. Sulsky, S.-J. Zhou, and H. L. Schreyer, Comput. Phys. Commun. **87**, 236 (1995).
[7] D. Sulsky and H. L. Schreyer, Comput. Methods Appl. Mech. Eng. **139**, 409 (1996).
[8] Allen R. York, Deborah Sulsky, and H. L. Schreyer, Int. J. Numer. Methods Eng. **44**, 1429 (1999).
[9] D. J. Evans and G. P. Morriss, *Statistical Mechanics of Nonequilibrium Liquids* (Academic, London, 1990).
[10] William G. Hoover, Phys. Rev. A **31**, 1695 (1985).
[11] Denis J. Evans and Brad Lee Holian, J. Chem. Phys. **83**, 4069 (1985).
[12] W. G. Hoover, A. J. C. Ladd, B. L. Holian, and R. B. Hickman, Phys. Rev. A **21**, 1756 (1980).
[13] W. G. Hoover, D. J. Evans, R. B. Hickman, A. J. C. Ladd, W. T. Ashurst, and B. Moran, Phys. Rev. A **22**, 1690 (1980).
[14] D. J. Evans, Mol. Phys. **47**, 1165 (1982); Andras Baranyai, Denis J. Evans, and Peter J. Daivis, Phys. Rev. A **46**, 7593 (1992); G. Ayton, O. G. Jepps, and D. J. Evans, Mol. Phys. **96**, 915 (1999); B. D. Todd, Denis J. Evans, and Peter J. Daivis, Phys. Rev. E **52**, 1627 (1995).
[15] G. Ayton and G. N. Patey, J. Chem. Phys. **102**, 9040 (1995).
[16] G. Ayton and G. N. Patey, Phys. Rev. Lett. **76**, 239 (1996).
[17] M. Houssa and Luis F. Rull, J. Chem. Phys. **109**, 9529 (1998).
[18] Julian T. Brown, M. P. Allen, E. Martin, and Enrique de Miguel, Phys. Rev. E **57**, 6685 (1998).
[19] M. A. Bates and G. R. Luckhurst, J. Chem. Phys. **110**, 7087 (1999).
[20] G. R. Luckhurst and G. Saielli, J. Chem. Phys. **112**, 4342 (2000).
[21] Douglas J. Cleaver, Christopher M. Care, Michael P. Allen, and Maureen P. Neal, Phys. Rev. E **54**, 559 (1996).
[22] S. W. de Leeuw, J. W. Perram, and E. R. Smith, Annu. Rev. Phys. Chem. **37**, 245 (1986); Proc. R. Soc. London, Ser. A **373**, 27 (1980).
[23] J. Alejandre, D. J. Tildesly, and G. A. Chapela, J. Chem. Phys. **102**, 4574 (1995).
[24] D. R. Wheeler, N. G. Fuller, and R. L. Rowley, Mol. Phys. **92**, 55 (1997).
[25] M. P. Allen and D. J. Tildesley, *Computer Simulation of Liquids* (Oxford Science, New York, 1987).
[26] Whether or not the system is in a liquid-crystalline or gel phase would require further experiments. For this work, the nonzero mean square displacement is sufficient.
[27] For reference the analytic solution for a massless spring with the same geometry and E has a total displacement of 0.009 mm.